Haptic Shared-Control Methods for Robotic Cutting under Nonholonomic Constraints

Rahaf Rahal, Firas Abi-Farraj, Paolo Robuffo Giordano, Claudio Pacchierotti

Haptic Shared-Control Methods for Robotic Cutting under Nonholonomic Constraints

Rahaf Rahal, Firas Abi-Farraj, Paolo Robuffo Giordano, Claudio Pacchierotti

***Abstract*— Robot-assisted cutting is considered an important task in several fields, such as robotic surgery, nuclear decommissioning, waste management, and manufacturing. Despite the complex dexterity requirements of cutting tasks, very simple mechanically-linked master-slave manipulators still dominate many of the above fields (e.g., nuclear robotics). Moreover, even when more dexterous manipulators are available (e.g., in robot-assisted surgery), the employed systems show little or no autonomy, delegating all control to the experience of the human operator. To ameliorate this situation, we present two haptic shared-control approaches for robotic cutting. They are designed to assist the human operator by enforcing different nonholonomic-like constraints representative of the cutting kinematics. To validate our approach, we carried out a human-subject experiment in a real cutting scenario. We compared our shared-control techniques with each other and with a standard haptic teleoperation scheme. Results show the usefulness of assisted control schemes in complex applications such as cutting. However, they also show a discrepancy between objective and subjective metrics.**

I. INTRODUCTION

Several solutions have been proposed for assisting a human operator in commanding complex robotic systems [1]–[4]. Among these solutions, shared control has proven to be an efficient tool for designing intuitive robotic teleoperation interfaces that help operators in carrying out increasingly difficult robotic tasks. Shared control makes it possible to *share* the available degrees of freedom of a robotic system between the operator and an autonomous controller, so as to facilitate the task for the human operator and improve the overall efficiency of the system [1], [2]. How to implement such division of roles between the human and the autonomous component highly depends on the task and robotic system [5], [6]. Nevertheless, different shared-control architectures have been proposed for different applications such as robotic grasping, cutting, and precise positioning [7]–[9].

Robotic cutting is particularly interesting for shared control, as it requires high dexterity and can have serious implications if it fails. It is in fact employed in various sensitive applications which range from surgical cutting [10] to nuclear decommissioning [11] and disaster response [12], [13]. Moreover, cutting applications feature a variety of constraints which can have a high impact on the task. For example, to avoid damaging the environment, the cutting tool should neither perform pure lateral motion nor rotate in place. Accounting for these constraints in the design of the control architecture can be key for a successful and safe task execution. Indeed, unicycle and car-like kinematic models have been used for modeling the cutting task to reflect its nonholonomic nature [14]–[16].

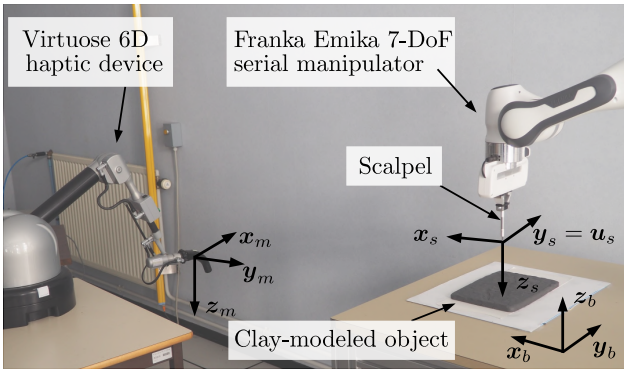

Fig. 1. Experimental setup and reference frames used for designing the shared-control techniques. Their objective is to help the operator cut the clay safely and intuitively. To do so, we enforced various nonholonomic-inspired constraints, limiting lateral motions, rotations in place, and sharp turns of the scalpel.

Several shared-control architectures have been proposed in the literature to tackle different cutting applications. For example, Prada and Payandeh [17] used geometric virtual fixtures for providing assistance during cutting. The user was guided towards a particular path using haptic feedback complemented with a visual interface. Experiments were performed in a virtual environment and no specific nonholonomic constraints were considered. Early work towards enforcing a nonholonomic behavior on robotic systems has also been proposed for cobots, where nonholonomy was ensured by mechanically limiting the DoF as to prevent any nonholonomic motion [18], [19]. The cobots then followed the forces applied by the human operator along the available DoF. However, most scenarios require more flexible and dexterous robots, capable of performing different tasks which may not always be nonholonomic. Enforcing nonholonomic constraints on multi-purpose robots through control has been tackled, for example, by Arai et al. [20]. The authors propose a robotic control architecture that helps a human operator in handling long objects by imposing virtual nonholonomic constraints. More recently, Li and Kazanzides [21] proposed a shared-control architecture for cutting in satellite servicing scenarios under time delay. The task consisted of cutting a straight line in multi-layer insulation (MLI) blankets (a thermal insulation patch used to cover satellites). A semi-autonomous architecture helped the operator in keeping the blade normal to the blanket. Vozar et al. [22] addressed a similar problem by designing four shared-control approaches.

R. Rahal is with Univ Rennes, Inria, CNRS, IRISA, Rennes, France. rahaf.rahal@irisa.fr

F. Abi-Farraj, P. Robuffo Giordano, and C. Pacchierotti are with CNRS, Univ Rennes, Inria, IRISA, Rennes, France. {firas.abi-farraj,prg,claudio.pacchierotti}@irisa.fr

The task again comprised cutting straight lines into MLI blankets under a time delay. In the first control approach, users were given control over all planar DoF. In the second one, lateral motion (away from the desired straight line) was scaled down to reduce its impact in comparison with the two other controlled DoF. In the third one, lateral motion was completely disregarded, i.e., the slave was forced to abide to nonholonomic constraints. In the fourth one, users were provided with visual guidance towards the desired straight line. In all modes, the master interface was free to move in any direction, and the constraints were implemented only at the slave side. The authors carried out a user study in which they compared the distance error over the trajectory, its "roughness," and the completion time. Results showed no significant differences between the four modalities.

While the approaches of [22] and [21] are promising, they mainly focus on treating the time delay in the system rather than the cutting task itself. In fact, they all consider rather simple cutting tasks (straight lines). In real scenarios, the cutting trajectories might be significantly more complicated and the environment considerably sturdier. Moreover, they provide the user with little information about the constraints being enforced. While the slave was constrained to a nonholonomic motion, this restriction was not reflected on the master interface, that was free to move in all directions. This mismatch between slave and master may create confusion and it might have been the reason for the limited improvements shown by these modalities.

This paper targets the limitations of the above-described architectures. It presents the design and evaluation of two shared-control approaches for commanding a torque-controlled manipulator in a cutting scenario. These approaches are designed to help the human operator complete the cutting task in an intuitive and safe way, by enforcing the constraints associated with the task itself, e.g., limiting lateral motions, rotations in place, and sharp turns of the tool. A key contribution of this paper is that the user is provided with information about the enforced nonholonomic constraints (alongside contact forces) via haptic feedback on the master device. The constraints at the master's side are imposed only using information from the master's position, limiting any unstable behavior due to communication delays between master and slave. We believe that this feedback is essential for the operator and can turn around the results of [22]. To evaluate our techniques, we carried out a human subject study with 12 users in a real cutting scenario. We compared the proposed shared-control approaches with each other and with a standard teleoperation scheme, analyzing five measures of performance.

II. Methods

The robotic system is composed of a master 6-DoF haptic interface and a slave 7-DoF torque-controlled manipulator, equipped with a scalpel. The environment is composed of a planar object to cut, placed on a table.

We consider three reference frames, shown in Fig. 1: $\mathcal{F}_s : \{\mathcal{O}_s, \boldsymbol{x}_s, \boldsymbol{y}_s, \boldsymbol{z}_s\}$, attached to the remote scalpel; $\mathcal{F}_m : \{\mathcal{O}_m, \boldsymbol{x}_m, \boldsymbol{y}_m, \boldsymbol{z}_m\}$, attached to the end-effector of the master interface; and $\mathcal{F}_b : \{\mathcal{O}_b, \boldsymbol{x}_b, \boldsymbol{y}_b, \boldsymbol{z}_b\}$, our base frame attached to the environment, i.e., the object to cut. The environment is assumed to be fixed and planar, with $\boldsymbol{z}_b$ being the normal to this plane. The scalpel ($\mathcal{F}_s$), as well as the end-effector of the master device ($\mathcal{F}_m$), are free to move along the three translational directions. However, their orientation is constrained via control, such that $\boldsymbol{z}_s = \boldsymbol{z}_m = -\boldsymbol{z}_b$. The system can thus only rotate around $\boldsymbol{z}_b$. This constraint is enforced in all the three control modalities described below.

Let $\boldsymbol{p}_s : (\boldsymbol{t}_s, \alpha_s) \in \mathbb{R}^4$ define the pose of the slave robot expressed in $\mathcal{F}_b$, where $\boldsymbol{t}_s \in \mathbb{R}^3$ encodes the three translational directions and $\alpha_s \in \mathbb{R}$ the rotation around $\boldsymbol{z}_b$. Similarly, let $\boldsymbol{p}_m : (\boldsymbol{t}_m, \alpha_m) \in \mathbb{R}^4$ define the pose of the master device expressed in $\mathcal{F}_b$. The master device is modeled as a generic (gravity pre-compensated) mechanical system,

$$\boldsymbol{M}_m(\boldsymbol{p}_m)\ddot{\boldsymbol{p}}_m + \boldsymbol{C}_m(\boldsymbol{p}_m, \dot{\boldsymbol{p}}_m)\dot{\boldsymbol{p}}_m = \boldsymbol{\tau}_m + \boldsymbol{\tau}_h, \quad (1)$$

where $\boldsymbol{M}(\boldsymbol{p}_m) \in \mathbb{R}^{4\times4}$ is the positive-definite and symmetric inertia matrix, $\boldsymbol{C}(\boldsymbol{p}_m, \dot{\boldsymbol{p}}_m) \in \mathbb{R}^{4\times4}$ accounts for Coriolis/centrifugal terms, and $\boldsymbol{\tau}_m, \boldsymbol{\tau}_h \in \mathbb{R}^4$ are the control and operator forces, respectively. Similarly, at the slave side,

$$\boldsymbol{M}_s(\boldsymbol{p}_s)\ddot{\boldsymbol{p}}_s + \boldsymbol{C}_s(\boldsymbol{p}_s, \dot{\boldsymbol{p}}_s)\dot{\boldsymbol{p}}_s = \boldsymbol{\tau}_s + \boldsymbol{\tau}_e, \quad (2)$$

where $\boldsymbol{M}(\boldsymbol{p}_s) \in \mathbb{R}^{4\times4}$ is the positive-definite and symmetric inertia matrix, $\boldsymbol{C}(\boldsymbol{p}_s, \dot{\boldsymbol{p}}_s) \in \mathbb{R}^{4\times4}$ accounts for Coriolis/centrifugal terms, and $\boldsymbol{\tau}_s, \boldsymbol{\tau}_e \in \mathbb{R}^4$ are the control and external forces, respectively.

We designed three different control approaches. The first one (T) is a simple human-in-the-loop teleoperation, with no added constraints related to the specificity of the cutting task. While this is a rather standard approach, we still deemed it important, as it still is the gold standard in many application scenarios, including robotic surgery. The second one (U) is a unicycle approach. It adds nonholonomic constraints to avoid any lateral motion of the knife tool, which may severely damage both the tool and the environment. However, this approach does not prevent the tool from rotating in place or performing sharp turns, which can also be dangerous. For this reason, we consider an additional mode C, in which the user has direct control over the radius of curvature of the trajectory, similar to the steering mechanism of a car. In addition to all the constraints enforced in U, this modality also ensures that the tool only rotates when a translation is commanded at the same time.

The general architecture of the system is summarized in Fig. 2. More details on each control mode are shown in Fig. 3 as well as in the video available as supplemental material and at https://youtu.be/DkW4OcjgX9M. We evaluated their performance against each other in the human subject study described in Sec. III.

A. Standard haptic teleoperation (condition T)

In this modality, the pose of the slave robot is linked to the pose of the master so as to replicate its motion. The manipulator receives torque commands that are calculated as

$$\boldsymbol{\tau}_s = \boldsymbol{K}\left(\boldsymbol{p}_{s,d} - \boldsymbol{p}_s\right) + \boldsymbol{D}\left(\dot{\boldsymbol{p}}_{s,d} - \dot{\boldsymbol{p}}_s\right), \quad (3)$$

where $\boldsymbol{p}_{s,d} = \boldsymbol{p}_m$ and $\dot{\boldsymbol{p}}_{s,d} = \dot{\boldsymbol{p}}_m$. $\boldsymbol{K} \in \mathbb{R}^{4\times4}$ is a proportional scaling term and $\boldsymbol{D} \in \mathbb{R}^{4\times4}$ is the corresponding derivative term. In our case, we choose $\boldsymbol{K}$ and $\boldsymbol{D}$ to be diagonal matrices with $\boldsymbol{K} = diag(500 \text{ N/m}, 350 \text{ N/m}, 150 \text{ N/m}, 15 \text{ Nm/rad})$ and $\boldsymbol{D} = diag(44 \text{ Ns/m}, 50 \text{ Ns/m}, 24 \text{ Ns/m}, 2 \text{ Nms/rad})$.

The external forces applied by the environment on the slave are fed back to the user through the master interface, such that

$$\boldsymbol{\tau}_m = \boldsymbol{\tau}_c + \boldsymbol{\tau}_{nc}, \tag{4}$$

where $\boldsymbol{\tau}_c$ represents the forces applied along the constrained directions, and $\boldsymbol{\tau}_{nc}$ the ones applied along the non-constrained directions. In this condition, since no constraints are added to the system, $\boldsymbol{\tau}_c = \boldsymbol{0}$ and $\boldsymbol{\tau}_{nc} = \boldsymbol{S}_x(\boldsymbol{\tau}_e - \boldsymbol{B}\dot{\boldsymbol{p}}_m)$, where $\boldsymbol{S}_x$ is a selection matrix projecting the force feedback on the non-constrained directions (the identity matrix in this case), and $\boldsymbol{B} \in \mathbb{R}^{4\times4}$ is a damping matrix which improves the bilateral stability of the system. We chose $\boldsymbol{B} = diag(4 \text{ Ns/m}, 4 \text{ Ns/m}, 4 \text{ Ns/m}, 0.05 \text{ Nms/rad})$ for a good trade-off between reactivity and stability (similarly to [23]).

B. Unicycle approach (condition U)

While T guarantees high flexibility, considering a cutting scenario enables us to introduce additional constraints which can make the teleoperation easier and safer. In particular, any pure lateral motion of the scalpel during cutting can induce significant damage on the material being cut (and even on the scalpel itself, if the material is hard enough). To limit this undesired behavior, we impose nonholonomic constraints on the robot motion, such that the scalpel is constrained to move along two translational directions only: *(i)* its cutting direction $\boldsymbol{u}_s$, and *(ii)* its vertical direction along $\boldsymbol{z}_b$. The scalpel can always rotate around its axis $\boldsymbol{z}_s$. In other words, it can move forward/backward, up/down, and rotate around its vertical axis; however, it cannot translate laterally, along the direction perpendicular to $\boldsymbol{u}_s$ and $\boldsymbol{z}_s$ (see Fig. 1). In our scenario, the scalpel was always oriented such that $\boldsymbol{u}_s = \boldsymbol{y}_s$.

To achieve this desired behavior, we constrain the master device such that the user is allowed to move along $\boldsymbol{x}_m$ and $\boldsymbol{z}_m$ in translation, as well as to rotate around $\boldsymbol{z}_m$. The motion around $\boldsymbol{y}_m$ is, however, blocked. To enforce this blockage, we define a plane $S_{l,m}(t) : (\boldsymbol{n}_{l,m}(t), \boldsymbol{t}_{l,m}(t))$, in which the motion of the master is constrained at any time t. $\boldsymbol{n}_{l,m}(t) \in \mathbb{R}^3$ is the normal vector to the plane, and $\boldsymbol{t}_{l,m}(t) \in \mathbb{R}^3$ is a point in space through which the plane passes. We can easily define $\boldsymbol{n}_{l,m}(t)$ as $\boldsymbol{n}_{l,m}(t) = [\boldsymbol{x}_m(t)]_x \boldsymbol{z}_m$, where $[\ ]_x$ is the skew symmetric operator. The definition of $\boldsymbol{t}_{l,m}(t) \in \mathbb{R}^3$ is, however, more tricky, as it is not only dependent on the current pose of the master device but also on its previous pose and can be defined as $\boldsymbol{t}_{l,m}(t) = \boldsymbol{t}_{l,m}(t-1) + (\boldsymbol{t}_m(t) - \boldsymbol{t}_m(t-1))\boldsymbol{x}_m$. Finally, the master interface is constrained to remain in the plane $S_{l,m}(t)$ by providing a linear force

$$\boldsymbol{\tau}_{l,m} = -K_{l,m} d_{l,m}(t) \boldsymbol{n}_{l,m}(t) - B_{l,m} \left(\dot{\boldsymbol{t}}_m \cdot \boldsymbol{n}_{l,m}(t)\right) \boldsymbol{n}_{l,m}(t), \tag{5}$$

where $d_{l,m}(t) = (\boldsymbol{t}_m - \boldsymbol{t}_{l,m}(t))\boldsymbol{n}_{l,}(t)$ is the distance between the current master pose and the plane $S_{l,m}(t)$, $K_{l,m} \in \mathbb{R}$ is a (high) stiffness parameter, and $B_{l,m} \in \mathbb{R}$ is the corresponding damping term. For our application, $K_{l,m} = 500$ N/m and $B_{l,m} = 16$ Ns/m.

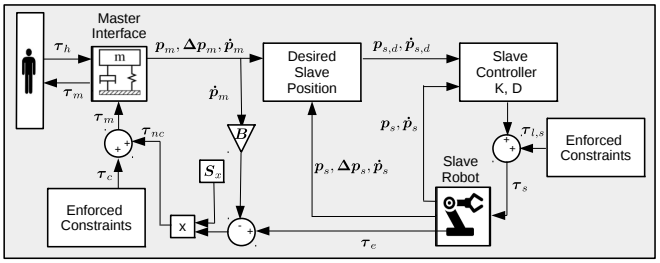

Fig. 2. Block diagram detailing the control architecture. In U and C, the *enforced constraints* intervene to account for the cutting task. In T, no constraint is enforced and therefore $\boldsymbol{\tau}_c = \boldsymbol{0}$ and $\boldsymbol{\tau}_{l,s} = \boldsymbol{0}$. In all conditions, along the non-constrained directions, the user receives haptic feedback reflecting the forces applied by the robot on the environment.

The linear motion along $\boldsymbol{x}_m$ is then mapped to the slave as a motion along the cutting direction of the scalpel $\boldsymbol{u}_s$, defining the new desired pose of the scalpel $\boldsymbol{p}_{s,d} : (\boldsymbol{t}_{s,d}, \alpha_{s,d})$ as

$$\boldsymbol{t}_{s,d}(t) = \underbrace{\begin{bmatrix} t_{sx}(t) \\ t_{sy}(t) \\ 0 \end{bmatrix} + d_{tot}(t)\boldsymbol{u}_s(t)}_{\text{planar motion}} + \underbrace{\begin{bmatrix} 0 \\ 0 \\ t_{mz}(t) \end{bmatrix}}_{\text{vertical motion}}, \tag{6}$$

where $\boldsymbol{t}_s(t) = [t_{sx}(t), t_{sy}(t), t_{sz}(t)]^T$, and $\boldsymbol{t}_m(t) = [t_{mx}(t), t_{my}(t), t_{mz}(t)]^T$. Moreover, $d_{tot}(t)$ is the total desired distance to be traveled by the slave robot at time t to match the change in position of the master. It is defined as $d_{tot}(t) = d_{tot}(t-1) + d_i(t)$, where $d_i(t)$ is the difference in the distance traveled by the master and slave in their last loop iteration,

$$d_i(t) = (\boldsymbol{t}_m(t) - \boldsymbol{t}_m(t-1))\,\boldsymbol{x}_m - (\boldsymbol{t}_s(t) - \boldsymbol{t}_s(t-1))\,\boldsymbol{u}_s. \tag{7}$$

This definition of $\boldsymbol{t}_{s,d}(t)$ ensures that the desired position of the slave is always along the pointing direction of the scalpel $\boldsymbol{u}_s$, guaranteeing the nonholonomic nature of the motion.

Forces $\boldsymbol{\tau}_s$ controlling the slave are then defined as

$$\boldsymbol{\tau}_s = \boldsymbol{K}(\boldsymbol{p}_{s,d} - \boldsymbol{p}_s) + \boldsymbol{D}(\dot{\boldsymbol{p}}_{s,d} - \dot{\boldsymbol{p}}_s) + \begin{bmatrix} \boldsymbol{\tau}_{l,s} \\ 0 \end{bmatrix}, \tag{8}$$

where $\boldsymbol{p}_{s,d} = [\boldsymbol{t}_{s,d}^T(t),\ \alpha_m]^T$, $\dot{\boldsymbol{p}}_{s,d} = [((\dot{\boldsymbol{p}}_m \boldsymbol{x}_m)\boldsymbol{u}_s + (\dot{\boldsymbol{p}}_m \boldsymbol{z}_m)\boldsymbol{z}_s)^T,\ \dot{\alpha}_m]^T$, and $\boldsymbol{\tau}_{l,s}$ is a lateral control force enforcing the nonholonomic motion constraints on the slave robot, defined similarly to $\boldsymbol{\tau}_{l,m}$ in (5),

$$\boldsymbol{\tau}_{l,s} = -K_{l,s} d_{l,s}(t) \boldsymbol{n}_{l,s}(t) - B_{l,s} \left(\dot{\boldsymbol{t}}_s \cdot \boldsymbol{n}_{l,s}(t)\right) \boldsymbol{n}_{l,s}(t), \tag{9}$$

where $S_{l,s}(t) : (\boldsymbol{n}_{l,s}(t), \boldsymbol{t}_{l,s}(t))$ is the plane we want to constrain the slave in, $d_{l,s}(t) = (\boldsymbol{t}_s - \boldsymbol{t}_{l,s}(t))\boldsymbol{n}_{l,s}(t)$ is the distance between the current slave pose and the plane $S_{l,s}(t)$, $K_{l,s} \in \mathbb{R}$ is a (high) stiffness parameter, and $B_{l,s} \in \mathbb{R}$ is the corresponding damping term. In our application, $K_{l,s} = 1000$ N/m and $B_{l,s} = 63$ Ns/m.

In addition to $\boldsymbol{\tau}_{l,m}$ imposing the constraints on the master interface ($\boldsymbol{\tau}_c = [\boldsymbol{\tau}_{l,m}, 0]^T$), the user also receives haptic feedback $\boldsymbol{\tau}_{nc}$ from the environment along the directions not constrained by the control, similarly to (4).

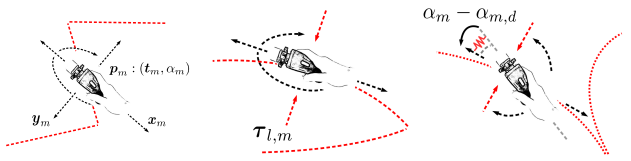

(T) Teleoperation. (U) Unicycle. (C) Car-like.

Fig. 3. Summary of the shared control modes. Black arrows are directions the user is allowed to control, red arrows directions which are blocked, dashed red lines sample trajectories. **(T) Teleoperation.** The user has control over all planar motions and the vertical movement. **(U) Unicycle.** Pure lateral motions are blocked. **(C) Car-like.** In addition to blocking the lateral motion, rotations in place and sharp turns are also avoided. The user controls the radius of curvature of the steering. A spring informs the user about the master position corresponding to a zero radius of curvature.

C. Car-like approach (condition C)

The previous approach prevents the user from moving the scalpel laterally. However, the user is still free to rotate it in place, which may also lead to significant damage of the tissue. Moreover, even when moving, it is important to limit the rate of rotation of the scalpel, as to avoid very sharp turns. To limit these undesired behaviors (i.e., rotating in place and hairpin bends), we impose additional constraints w.r.t. the control discussed in Sec. II-B, executing rotations only if the slave moves along $\boldsymbol{u}_s$. Moreover, in this approach, the user is given control over the radius of curvature of the trajectory, R_d. Similarly to driving a car, the user does not directly control the angular velocity of the slave but rather the steering angle.

As in Sec. II-B, we constrain the master interface such that the user is allowed to move along $\boldsymbol{x}_m$ and $\boldsymbol{z}_m$, with a hard spring blocking any lateral motion. Considering rotations, a soft spring is applied around $\boldsymbol{z}_m$ so as to fix the orientation of the master device at a particular pivot angle $\alpha_{m,d}$ (defined in the coming lines). As the user drives the master device away from $\alpha_{m,d}$, this divergence $(\alpha_m - \alpha_{m,d})$ is mapped as the desired radius of curvature of the trajectory R_d (i.e., the desired steering rate), such that

$$R_d = \frac{k}{(\alpha_m - \alpha_{m,d})^n}, \tag{10}$$

where $k \in \mathbb{R}$ and $n \in \mathbb{R}$ are control gains. In this work, after pilot tests, we empirically chose $k = 1/40$ and $n = 2$.

Then, the angular velocity of the slave, $\dot{\alpha}_s$, is designed to ensure that the curvature of the trajectory follows R_d when the user commands a linear velocity along $\boldsymbol{u}_s$, such that

$$\dot{\alpha}_{s,d} = sgn(\alpha_m - \alpha_{m,d}) \frac{|\dot{\boldsymbol{t}}_m \cdot \boldsymbol{x}_m|}{R_d}. \tag{11}$$

This technique ensures that the slave tool does not rotate in place, but it only rotates when a linear motion is commanded. Moreover, it also ensures that the motion of the slave follows the desired commanded radius of curvature, R_d.

The pivot master device angle $\alpha_{m,d}$ is updated at every iteration to account for $\dot{\alpha}_s$ and to ensure that the master and the slave are aligned at all times,

$$\alpha_{m,d}(t) = \alpha_{m,d}(t-1) + \dot{\alpha}_{s,d}\Delta t. \tag{12}$$

A similar integrator is used to retrieve the desired orientation $\alpha_{s,d}(t)$ of the slave, which is then commanded as in (8), now with $\boldsymbol{p}_{s,d} = [\boldsymbol{t}_{s,d}^T(t),\ \alpha_{s,d}]^T$ and $\dot{\boldsymbol{p}}_{s,d} = [((\dot{\boldsymbol{t}}_m \boldsymbol{x}_m)\boldsymbol{u}_s + (\dot{\boldsymbol{t}}_m \boldsymbol{z}_m)\boldsymbol{z}_s)^T,\ \dot{\alpha}_{s,d}]^T$.

As before, similarly to (4), the user receives $\boldsymbol{\tau}_{nc}$ along the directions not constrained by the control. And $\boldsymbol{\tau}_c = [\tau_{l,m}, 0]^T + K_{z_m}(\alpha_{m,d} - \alpha_m)[0\ 0\ 0\ 1]^T - B_{z_m}\dot{\alpha}_m[0\ 0\ 0\ 1]^T$, where $K_{z_m} = 1.2$ Nm/rad is a stiffness constant and $B_{z_m} = 0.12$ Nms/rad a damping constant.

III. Experimental evaluation

To evaluate the effectiveness and viability of our shared-control approaches, we carried out a human subject experiment.

A. Setup

The experimental setup is shown in Fig. 1, and it is described at the beginning of Sec. II. The master side consisted of a Haption Virtuose 6-DoF haptic grounded interface. The slave side consisted of a Franka Panda 7-DoF serial manipulator equipped with a scalpel. The remote environment was composed of a 25×17×1.5 cm surface made of modeling clay. To enable the operator to see the environment, the master interface was placed next to the slave robot.

B. Task and Conditions

Participants used the master interface to control the motion of the slave manipulator. The task consisted in cutting a target shape into the modeling clay. Participants were asked to complete the cutting task as precisely and fast as possible. Before each repetition, the experimenter used a pre-prepared plastic mold to draw the target shape on the clay, to make it visible to the user but without introducing any deformation to the material. The task started when the manipulator touched the clay for the very first time and it was considered completed when the shape was totally carved (i.e., when the scalpel reached the end of the drawn shape). Participants were only allowed one pass on the shape. The task, environment, and target shapes have been chosen following a discussion with clinicians, which considered them as good representatives of surgical incisions [10]. The setup also reminds scenarios of sort and segregation of radioactive waste [24], where teleoperated robots are used to cut open old containers and sort the waste according to its radioactivity level.

We consider different ways of commanding the motion of the robot through the haptic interface: (T) standard teleoperation, (U) unicycle approach, and (C) car-like approach. See Sec. II for details on these control techniques.

For each control condition, participants were asked to carve three different shapes:

- L: a straight line, resembling sternotomy or upper midline incisions;
- B: a bent line, resembling Gibson, inguinal or femoral incisions;
- S: a sinusoidal shape, resembling Clamshell or sinusoidal coronal incisions;

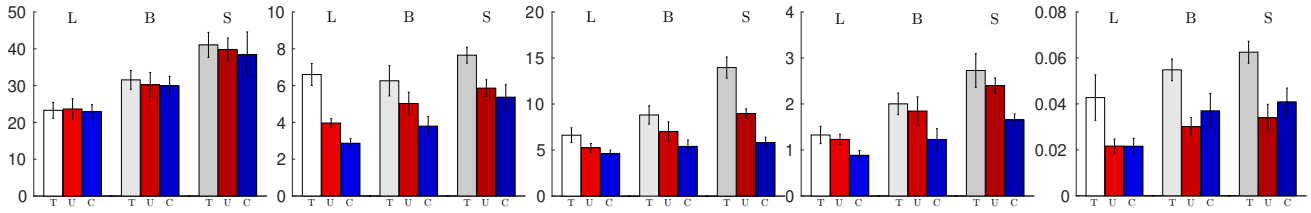

Fig. 4. Human subjects experiment. Objective metrics. Mean and standard error of the mean of (a) completion time, (b) error in carving the target shape, (c) max lateral force, (d) mean lateral force, and (e) roughness of the cut profile for the three control conditions (T, U, C) and the three target shapes (L, B, S).

Each subject carried out twelve randomized repetitions of the cutting task, one for each control condition and shape. Trials were randomized to avoid any learning effect. A video presenting the experiment and showing representative trials in the different conditions is available as supplemental material and at https://youtu.be/DkW4OcjgX9M.

C. Participants

Twelve subjects (average age 26.6, 8 males, 4 females) participated in the study. Four of them had previous experience with haptic interfaces. The experimenter explained the procedures and spent about one minute adjusting the setup to make it comfortable for the subject before beginning the experiment. Each subject then spent about two minutes practicing the control of the telemanipulation system before starting the experiment.

D. Results

To evaluate the effectiveness of our system in cutting the considered shapes and the usefulness of the proposed shared-control approaches, we recorded *(i)* the completion time, *(ii)* the error in following the target trajectory, *(iii-iv)* the maximum and mean lateral force applied by the scalpel on the environment, and *(v)* a measure of "roughness" of the cut profile. The latter indicates how clean the trajectory is from irregularities and bends. Details on the calculation of these metrics are given below. To compare the metrics, we ran two-way repeated-measures ANOVA tests on the data. The control modality (T vs. U vs. C) and target shape (L vs. B vs. S) were treated as within-subject factors. All data passed the Shapiro-Wilk normality test. A Greenhouse-Geisser correction was used when the assumption of sphericity was violated. Results of post hoc analysis with Bonferroni adjustments or simple main effects are reported in Table I (only significant p values are shown).

Figure 4a shows the completion time, $t_f - t_i$, averaged across user trials. It is calculated as the time elapsed between the instant t_i the manipulator touches the clay for the first time and the instant t_f the shape is completely carved. Mauchly's Test of Sphericity indicated that the assumption of sphericity had been violated for the shape variable ($\chi^2(2) = 8.242, p = 0.016$). The two-way repeated-measure ANOVA revealed no statistically significant change for this metric across control conditions (F(2, 22) = 0.122, $p > 0.05$), but it showed a statistically significant change across target shapes (F(1.281, 14.090) = 26.831, $p < 0.001$). Figure 4b shows the mean

TABLE I

SUMMARY OF THE EXPERIMENT

Task	Control the haptic-enabled teleoperation system to cut a target shape into modeling clay (12 subjects enrolled).
Conditions	Control approaches T (standard teleop.), U (unicycle-like), C (car-like) Target shapes L (straight line), B (bent line), S (sinusoidal shape)

Statistical analysis (two-way repeated-measure ANOVA, a = 0.05)

Completion time			
Main effect of target shape			
L vs. B	$p = 0.001$	B vs. S	$p = 0.006$
L vs. S	$p < 0.001$		
Error			
Main effect of control approach			
T vs. U	$p = 0.022$	U vs. C	$p = 0.016$
T vs. C	$p = 0.002$		
Main effect of target shape			
L vs. S	$p = 0.002$		
Max. lateral force			
Simple main effect of control approach (condition/shape)			
T/B vs. C/B	$p = 0.040$	T/S vs. C/S	$p < 0.001$
T/S vs. U/S	$p = 0.025$		
Simple main effect of target shape (shape/condition)			
L/T vs. S/T	$p = 0.001$	L/U vs. S/U	$p < 0.001$
B/T vs. S/T	$p = 0.014$		
Mean lateral force			
Main effect of control approach			
T vs. C	$p = 0.004$	U vs. C	$p = 0.003$
Main effect of target shape			
L vs. B	$p = 0.034$	L vs. S	$p < 0.001$
Roughness			
Main effect of control approach			
T vs. U	$p = 0.001$	T vs. C	$p = 0.025$
Main effect of target shape			
L vs. B	$p = 0.003$	L vs. S	$p = 0.006$

error in following the target shape, averaged across trials. It is calculated as the mean distance between the profile cut by the user and the target shape, i.e., $(\sum_{k=1}^{N} \boldsymbol{t}_s(k) - \boldsymbol{t}_s^*(k))/N$, where $\boldsymbol{t}_s^*(k)$ is the closest point to $\boldsymbol{t}_s(k)$ on the target shape and N is the number of sample points in the user-cut trajectory. Mauchly's Test of Sphericity indicated that the assumption of sphericity had been violated for the control variable ($\chi^2(2) = 6.843, p = 0.033$) and for the interaction between variables ($\chi^2(9) = 30.031, p = 0.001$). The two-way repeated-measure ANOVA revealed statistically significant change for this metric across control conditions (F(1.337, 14.710) = 16.556, $p = 0.001$) and target shapes (F(2, 22) = 8.281, $p = 0.002$). Figure 4c shows the maximum lateral force, averaged across trials. It is calculated as the maximum

value of force sensed by the robot along the axis $\boldsymbol{x}_s$, which is perpendicular to the scalpel motion. Since moving the scalpel laterally with respect to its direction of motion can damage the tissue, this force should be as small as possible. Data passed the Mauchly's Test of Sphericity. The two-way repeated-measure ANOVA revealed a statistically significant change for this metric across control conditions (F(2, 22) = 23.131, $p < 0.001$) and target shapes (F(2, 22) = 25.873, $p < 0.001$). There was also a statistically significant two-way interaction between shapes and control conditions (F(4, 44) = 5.075, $p = 0.002$). Figure 4d shows the mean lateral force, averaged across trials. It is calculated as the mean value of force sensed by the robot along $\boldsymbol{x}_s$. As above, this force should be as small as possible. Mauchly's Test of Sphericity indicated that the assumption of sphericity had been violated for the interaction between variables ($\chi^2(9) = 17.675, p = 0.042$). The two-way repeated-measure ANOVA revealed a statistically significant change for this metric across control conditions (F(2, 22) = 10.208, $p = 0.001$) and target shapes (F(2, 22) = 14.085, $p < 0.001$). Figure 4e shows a measure of "roughness" of the cut, averaged across trials. It is calculated as the mean difference between the profile carved by the user and the same profile smoothed using a low-pass Butterworth zero-phase digital filter [25], i.e., $(\sum_{k=1}^{N} \boldsymbol{t}_s(k) - \boldsymbol{t}_{s_{filt}}(k))/N$, where $\boldsymbol{t}_{s_{filt}}(k)$ is the closest point to $\boldsymbol{t}_s(k)$ on the filtered trajectory. Mauchly's Test of Sphericity indicated that the assumption of sphericity had been violated for the interaction between variables ($\chi^2(9) = 17.225, p = 0.048$). The two-way repeated-measure ANOVA revealed a statistically significant change for this metric across control conditions (F(2, 22) = 14.233, $p < 0.001$) and target shapes (F(2,22) = 13.200, $p < 0.001$).

Finally, eight subjects out of twelve found control condition U to be the most effective at completing the cutting task. Three subjects preferred condition T while one preferred C.

IV. Discussion and Conclusions

This paper presented the design and evaluation of two shared-control approaches for assisting a human operator in various robot-assisted cutting tasks.

The first shared-control technique resembled the behavior of a unicycle (U). We imposed nonholonomic constraints on the motion of the robotic system, such that the scalpel translation was limited to its cutting direction (forward/backward) and its vertical direction (up/down). These constraints prevented the operator from inadvertently applying high lateral forces during the cutting, which would result in dangerous ruptures of the environment. Although effective, in this condition the operator was still able to rotate the scalpel in place, which could also lead to significant damage. For this reason, we designed an additional shared-control techniques (C), enforcing an additional constraint on the unicycle motion that ensured the scalpel rotation was coupled with a linear motion.

To validate our approach, we carried out a human-subject experiment in a real cutting scenario, considering the two shared-control techniques (U, C) as well as a standard teleoperation approach (T). We included the standard teleoperation approach because it is still largely used in many application scenarios, including robot-assisted surgery. The task consisted in cutting a target shape into a piece of modeling clay. We considered three shapes of increasing complexity: a straight line (L), a bent line (B), and a sinusoidal shape (S).

Results show that the three proposed shared-control approaches significantly outperform standard teleoperation in most metrics. Specifically, C outperformed T in all metrics but completion time, and U outperformed T in all metrics but completion time and mean lateral force. These results are sustained across the three considered shapes (see Table I). This proves our hypothesis that shared control can be a viable and effective approach to improve currently-available teleoperation systems for cutting tasks, which is in agreement with previous results in the literature. Comparing performance among the proposed shared-control techniques (U vs. C), we can see that limiting the maximum radius of curvature and preventing rotations in place (C) significantly lowers the lateral forces w.r.t. U, where these constraints were not enforced. Moreover, the error metric shows significant differences among all pairs, ranking C first (lowest error), followed by U and T (highest error). This latter result is partially in contrast with that of Vozar et al. [22], where imposing a virtual nonholonomic constraint on the end-effector motion did not significantly reduce the error in cutting a target path. However, Vozar et al. [22] did not use haptic feedback to inform the users about the constraints and carried out their experiment under a 4s delay. Finally, comparing performance among the target shapes, we can see that, as the shapes become more complex, their performance degrades. It is also interesting to notice that, for most metrics, as the shapes become more complex, the difference of T vs. U and C increases. This result is quite expected, as users need more help when cutting more complex shapes.

Surprisingly, the subjective metrics did not always agree with the above results. In fact, users preferred T and U over C. Indeed, the many constraints imposed in the C modality created the impression of conditions difficult to use. A common comment among subjects was that they often felt "limited" when using C, and that T and U made them feel "more in control" of the slave robot. However, it is important to notice that none of our subjects was experienced in using the experimental setup. In fact, the recorded subjective results might change in the presence of experienced users. This is something we plan to extensively study in the coming future, since all the operators in our target scenarios are skilled and experienced (e.g., surgeons). Another aspect to consider is the amount of information provided to the users. Although we took time to explain the procedure and the conditions, a more detailed explanation of how the shared control works and why it is important for certain applications might have led to a deeper understanding and acceptance by the users, who seemed overly reluctant to relinquish control.

Two sources of potential instability are present in the system, corresponding to the two sources of force feedback: $\boldsymbol{\tau}_c$, which imposes the nonholonomic constraints, and $\boldsymbol{\tau}_{nc}$, which reflects the interaction of the slave with the environment. However, $\boldsymbol{\tau}_c$ raises no concern, as the constraints enforced

at the master side are evaluated from the pose of the master interface only. This design allowed the use of high stiffness parameters ($K_{l,m} = 500$ N/m). On the other hand, since we experienced very small communication delays in our setup, a damping matrix was sufficient to avoid any undesired oscillation resulting from $\boldsymbol{\tau}_{nc}$. However, in cases where communication delays might be significant (e.g., space operations, remote robot-assisted surgery), stability could be enforced via passivity [26]. We plan to study in the future the effect of time delays on the performance of haptic shared control techniques.

Finally, since we are using *kinesthetic* haptic feedback, we are limiting the control capabilities of the human users, who are not able to freely move the robot wherever they prefer. To address this point, we are studying new ways of providing guidance information to the operators using *only* ungrounded haptic stimuli, with the objective of providing the users with information about what the controller thinks they should do, but without reducing their capabilities to control the motion of the robot. A possible approach is to employ a wearable device instead of the grounded Virtuose interface, as done in [27]–[29]. This point is important in our target scenarios, where it is paramount to value the knowledge and experience of our operators. In the future, we are also planning to study how the strength of haptic constraints affects the task performance, e.g., a system could use stiff constraints (i.e., less freedom for the operator) when it is operated by novices, while it could implement soft constraints (i.e., more freedom for the operator) when it is operated by experts. This flexible approach could be also useful when teaching new operators, employing different levels of autonomy according to the operator's experience. We also plan to carry out more human subject experiments in real scenarios, tailored for specific applications (e.g., cutting real tissue) and considering changes in other variables (e.g., different stiffness of the environment, communication delays, quality of the visual feeback). Finally, we will test the effectiveness of the proposed approaches against other (shared) control techniques.

REFERENCES

[1] D. A. Abbink, M. Mulder, and E. R. Boer, "Haptic shared control: smoothly shifting control authority?" *Cognition, Technology & Work*, vol. 14, no. 1, pp. 19–28, 2012.

[2] T. B. Sheridan, "Human-robot interaction: Status and challenges," *Human Factors*, vol. 58, no. 4, pp. 525–532, 2016, pMID: 27098262.

[3] P. F. Hokayem and M. W. Spong, "Bilateral teleoperation: An historical survey," *Automatica*, vol. 42, no. 12, pp. 2035 – 2057, 2006.

[4] C. Pacchierotti, F. Ongaro, F. Van den Brink, C. Yoon, D. Prattichizzo, D. H. Gracias, and S. Misra, "Steering and control of miniaturized untethered soft magnetic grippers with haptic assistance," *IEEE Transactions on Automation Science and Engineering*, vol. 15, no. 1, pp. 290–306, 2017.

[5] R. Groten, D. Feth, H. Goshy, A. Peer, D. A. Kenny, and M. Buss, "Experimental analysis of dominance in haptic collaboration," in *Proc. IEEE Intl. Symp. on Robot and Human Interactive Communication*, Sep. 2009, pp. 723–729.

[6] K. B. Reed and M. A. Peshkin, "Physical collaboration of human-human and human-robot teams," *IEEE Trans. Haptics*, vol. 1, no. 2, pp. 108–120, 2008.

[7] J. Kofman, X. Wu, T. J. Luu, and S. Verma, "Teleoperation of a robot manipulator using a vision-based human-robot interface," *IEEE Trans. Industrial Electronics*, vol. 52, no. 5, pp. 1206–1219, 2005.

[8] M. Selvaggio, F. Abi-Farraj, C. Pacchierotti, P. Robuffo Giordano, and B. Siciliano, "Haptic-based shared-control methods for a dual-arm system," *IEEE Robotics and Automation Letters*, vol. 3, no. 4, pp. 4249–4256, 2018.

[9] F. Abi-Farraj, C. Pacchierotti, O. Arenz, G. Neumann, and P. Robuffo Giordano, "A haptic shared-control architecture for guided multi-target robotic grasping," *IEEE Trans. Haptics*, pp. 1–1, 2019.

[10] V. Patnaik, R. K. Singla, and V. Bansal, "Surgical incisions—their anatomical basis part iv-abdomen," *Journal of the Anat. Soc. India*, vol. 50, no. 2, pp. 170–8, 2001.

[11] Y. S. Park, H. Kang, T. F. Ewing, E. L. Faulring, J. E. Colgate, and M. A. Peshkin, "Enhanced teleoperation for d and d," in *Proc. IEEE Int. Conf. Robotics and Automation*, vol. 4, 2004, pp. 3702–3707 Vol.4.

[12] M. DeDonato et al., "Human-in-the-loop control of a humanoid robot for disaster response: A report from the darpa robotics challenge trials," *J. Field Robotics*, vol. 32, no. 2, pp. 275–292, 2015.

[13] F. Abi-Farraj, B. Henze, A. Werner, M. Panzirsch, C. Ott, and M. A. Roa, "Humanoid teleoperation using task-relevant haptic feedback," in *IEEE/RSJ Intl. Conf. Intell. Robots and Systems*, 2018, pp. 5010–5017.

[14] G. Campion, B. d'Andrea Novel, and G. Bastin, "Controllability and state feedback stabilizability of non holonomic mechanical systems," in *Advanced Robot Control*, C. Canudas de Wit, Ed., 1991, pp. 106–124.

[15] A. M. Bloch, M. Reyhanoglu, and N. H. McClamroch, "Control and stabilization of nonholonomic dynamic systems," *IEEE Trans. Automatic Control*, vol. 37, no. 11, pp. 1746–1757, 1992.

[16] H. McClamroch, M. Reyhanoglu, and M. Rehan, "Knife-edge motion on a surface as a nonholonomic control problem," *IEEE Control Systems Letters*, vol. 1, no. 1, pp. 26–31, 2017.

[17] R. Prada and S. Payandeh, "A study on design and analysis of virtual fixtures for cutting in training environments," in *Proc. World Haptics Conference*, March 2005, pp. 375–380.

[18] R. B. Gillespie, J. E. Colgate, and M. A. Peshkin, "A general framework for cobot control," *IEEE Trans. Robotics and Automation*, vol. 17, no. 4, pp. 391–401, 2001.

[19] C. A. Moore, M. A. Peshkin, and J. E. Colgate, "Cobot implementation of virtual paths and 3d virtual surfaces," *IEEE Trans. Robotics and Automation*, vol. 19, no. 2, pp. 347–351, 2003.

[20] H. Arai, T. Takubo, Y. Hayashibara, and K. Tanie, "Human-robot cooperative manipulation using a virtual nonholonomic constraint," in *Proc. IEEE Intl. Conf. Robotics and Automation*, vol. 4, 2000, pp. 4063–4069 vol.4.

[21] X. Li and P. Kazanzides, "Task frame estimation during model-based teleoperation for satellite servicing," in *Proc. IEEE Intl. Conf. Robotics and Automation*, 2016, pp. 2834–2839.

[22] S. Vozar, Z. Chen, P. Kazanzides, and L. L. Whitcomb, "Preliminary study of virtual nonholonomic constraints for time-delayed teleoperation," in *Proc. IEEE/RSJ Intl. Conf. Intell. Robots and Systems*, 2015, pp. 4244–4250.

[23] F. Abi-Farraj, C. Pacchierotti, and P. Robuffo Giordano, "User evaluation of a haptic-enabled shared-control approach for robotic telemanipulation," in *Proc. IEEE/RSJ Intl. Conf. Intell. Robots and Systems*, 2018, pp. 1–9.

[24] N. Marturi, A. Rastegarpanah, C. Takahashi, M. Adjigble, R. Stolkin, S. Zurek, M. Kopicki, M. Talha, J. A. Kuo, and Y. Bekiroglu, "Towards advanced robotic manipulation for nuclear decommissioning: A pilot study on tele-operation and autonomy," in *Proc. Int. Conf. Robotics and Automation for Humanitarian Applications*, 2016, pp. 1–8.

[25] E. Gadelmawla, M. Koura, T. Maksoud, I. Elewa, and H. Soliman, "Roughness parameters," *Journal of Mat. Process. Tech.*, vol. 123, no. 1, pp. 133–145, 2002.

[26] D. Lee and K. Huang, "Passive-set-position-modulation framework for interactive robotic systems," *IEEE Trans. on Robotics*, vol. 2, no. 26, pp. 354–369, 2010.

[27] F. Chinello, C. Pacchierotti, J. Bimbo, N. G. Tsagarakis, and D. Prattichizzo, "Design and evaluation of a wearable skin stretch device for haptic guidance," *IEEE Robotics and Automation Letters*, vol. 3, no. 1, pp. 524–531, 2018.

[28] J. Bimbo, C. Pacchierotti, M. Aggravi, N. Tsagarakis, and D. Prattichizzo, "Teleoperation in cluttered environments using wearable haptic feedback," in *IEEE/RSJ Intl. Conf. Intell. Robots and Systems*, 2017, pp. 3401–3408.

[29] M. Aggravi, F. Pausé, P. Robuffo Giordano, and C. Pacchierotti, "Design and evaluation of a wearable haptic device for skin stretch, pressure, and vibrotactile stimuli," *IEEE Robotics and Automation Letters*, vol. 3, no. 3, pp. 2166–2173, 2018.